RESEARCH PAPER

The Austempering Kinetics, Microstructural Development, and Processing Window in the Austempered, Fe-3.2C-4.8Al Compacted Graphite Cast Iron

A. Kazazi[1], S. M. Montazeri[1] and S. M. A. Boutorabi[2*]

* boutorabi@iust.ac.ir

[1] Department of Material Science and Technology, Sharif University of Technology, Tehran, Iran
[2] School of Metallurgy and Materials Engineering, Iran University of Science and Technology, Tehran, Iran

Abstract: In the present study, austempering heat treatment was performed on compacted graphite aluminum cast iron with the chemical composition of 4.8 wt% Al, 3.2 wt% C, 0.81 wt% Ni, 0.37 wt% Mn, and 0.02 wt% Mg. This study aims to investigate the effect of aluminum additions and removal of silicon on the kinetics of austempering transformation of Fe-3.2%C alloy. The cast samples were austenitized at 900 ℃ for 120 min and the isothermal austempering heat treatment was performed at 200 ℃, 300 ℃, and 400 ℃ for 5, 30, 60, 120, and 180 minutes, respectively. The kinetics of this transformation was studied by X-ray diffraction (XRD) analysis. The effect of temperature and time on the microstructure and hardness of the austempered samples was investigated and discussed. The presence of Al was seen to the prolonged form of the carbides from high carbon austenite, and that expanded the process window in the austempering transformation. Besides, the lower bainitic ferrite phase was observed in the austempered samples at 200 ℃ and 300 ℃. Increasing austempering temperature to 400 ℃ changed the lower bainite to the upper bainite structure. The volume fraction of austenite reached its maximum level (34.6 %) after austempering the samples at 400 ℃ for 30 minutes.

Keywords: austempering kinetic, compacted graphite, aluminum cast iron, ferritic bainite, window process.

1. INTRODUCTION

The idea of using aluminum instead of silicon was suggested first in the early twentieth century [1, 2]. The idea thereinafter was followed up by some studies (Defrancq [3] and Boutorabi [4]). The outcomes of these examinations were the development of a new family of the cast irons. This new category of cast-iron has several advantages over conventional types, such as higher tensile strength, enhanced thermal shock resistance, good thermal conduction at high temperatures, and also higher graphitization at lower casting modulus [2, 5].

Aluminum-alloyed cast irons have unique specifications, such as high-temperature oxidation resistance, improved machinability, enhanced strength at room and elevated temperatures, and good sound-damping capacity. Turbocharger diesel engine block, the brake discs, brake bowl of the cars, cylinder head, cylinder liner of the motor, camshaft, turbine exhaust diffuser, and ring piston are the examples of industrial parts that have been made partly or entirely from aluminum cast iron [2, 6, 7].

By using Al instead of Si in cast irons, the weight of produced parts can be reduced, and because of the higher graphitization ability of Al compare with Si, the thin-wall castings can be produced without the formation of the eutectic carbide [2, 8]. Consequently, amounts of the Fe_xC_y carbide in aluminum cast iron are lower than silicon cast iron. Besides, the Fe_3AlC_x carbides that cause brittleness and also reduce machinability of cast iron have not been observed in Al cast irons with up to 6.8 wt% Al [9].

The austempering of Al cast iron at the first stage (after passing austenite temperature to the austempering temperature range) begins by creating a somewhat stable combination of high carbon austenite and acicular ferrite (or ferrite + carbide). Graphitizing elements such as silicon and aluminum, due to their effect on preventing carbide formation, let the transformation products (ferrite or ferrite + carbide) nucleates at or near graphite nodules followed by growth into the austenite matrix [10-18].

At the second stage, eventually, the high carbon austenite begins to transform to its more stable products of acicular ferrite and carbide followed by a steady decrease in the volume fraction of high carbon austenite. This stage will continue until the amount of carbon reaches a stable level

[11-13]. Carbides can nucleate in acicular ferrite, or at the interface of acicular ferrite and reacted stable austenite. The interface between carbides and the matrix is coherent [14, 15].

The main difference between the austempering process of Fe-C-Si and Fe-C-Al cast iron is the effect of Al on the second stage and the fact that carbide precipitation shifts to longer austempering times. Thus, the addition of alloying elements delays the onset of the second stage, thereby increasing the possibility of generating stable high carbon austenite. Studies have shown that the amount of carbides is reduced by adding Al, which also results in increased relative elongation [1, 7, 11].

The values obtained in austempered compacted graphite cast iron (CG cast iron) were higher with respect to austempered ductile iron (ADI), corroborating the faster kinetics in CG cast Iron. In fact, presenting more nucleation sites for the ferrite needles nucleation in CG cast iron favors the kinetics [16].

According to our knowledge, the austempering transformation of 4.8 % Al compacted graphite cast iron has not been studied until now. This study aims to introduce the modern austempered Al-containing compacted graphite cast iron with proper mechanical properties and enlarged window process. Accordingly, the austempering transformation was studied for a 4.8 %-Al-containing CG iron under different isothermal holding times and temperatures. The effects of adding Al instead of Si in the chemical composition of Fe-3.2%C on the microstructure, the volume fraction of formed phases, hardness, and window process were also investigated.

2. EXPERIMENTAL PROCEDURE

The mold was made from silica sand (AFS grain fineness 60) and bonded with 3 % of the resin. Sand molds were obtained from 50 mm length and 20 mm width fluidity belt pattern. A base metal of composition 0.2 C, 0.29 Si, 0.5 Mn, 0.03 P, 0.04 S was used to produce CG cast iron in a 20 kg medium frequency induction furnace for one

hour at a temperature range of 1480-1500 ˚C. Then 0.04 wt% of the aluminum was added to the melt at a temperature of 1350 ˚C. The remaining aluminum was added to the melt by the plunging method. Before pouring the melt into the crucible, the melting temperature was raised to about 1530-1535 ˚C. Finally the necessary amount of $NiMg_{15}$ and tin were added to the ladle to obtain CG morphology. The Mg treated melt was inoculated by 0.02 wt% Zircinoc and 0.02 wt% Superseed and cast in the mold cavity.

The chemical composition of the melt is presented in Table 1. The dimensions of the samples were about $20\times20\times15$ mm^3.

To perform and austenitize the austempering heat treatment, sixteen samples were placed in a heat treatment furnace at 900 ˚C for 120 minutes. One of the samples was immediately cooled in water. Other samples were rapidly transferred to the molten salt bath. The austempering process was performed in the molten salt bath at temperatures of (200 ˚C, 300 ˚C, and 400 ˚C) for 5, 30, 60, 120, and 180 minutes.

The heat treatment furnace was an electrical resistance type one with a capacity of 11 liters and a temperature accuracy of ±2 ˚C. The salt bath consisted of 55 wt% $NaNO_2$ and 45 wt% KNO_3. After the austempering of samples, all of them were air-cooled. To prepare the samples for investigation by optical and scanning electron microscopy, the metallography treatments were done based on the ASTM E 3-01 metallography and ASTM E 407-99 metals micro-etch standards. The samples were etched using a 5% Nital solution for 5 to 70 seconds.

To measure the hardness of the samples, the hardness technique under a load of 150 kg according to ASTM E 10-15 was used. The average of three measurements was reported as the hardness of each sample.

Eventually, the X-ray diffraction (XRD) method was used to determine the volume fraction of formed phases and measure some parameters such as the carbon content of the retained austenite.

Table 1. Chemical composition of the Al compacted graphite cast iron (wt %)

S	P	Sn	Cr	Ni	Mn	Mg	Si	Al	C	Fe	Element
0.022	0.023	0.17	0.11	0.81	0.37	0.02	0.28	4.8	3.2	Base	As cast base metal

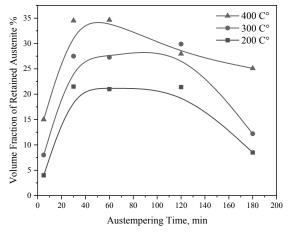*A. Kazazi, S. M. Montazeri and S. M. A. Boutorabi*

3. RESULTS AND DISCUSSION

3.1. Process window

Due to the high nucleation rate of ferrite from austenite, the first step austempering takes place more rapidly in cast iron containing Al compared with Si cast iron. Besides, the higher graphitization ability of Al in comparison with Si and also higher absorption of carbon in the austenite lead to a longer process window in Al cast irons.

The energy resulting from the supercooling (temperature difference between eutectic and austempering temperatures) acts as the driving force for ferrite nucleation in austenite. The advantage of Al compared to Si is its effect on further increasing the eutectic temperature. Hence, the driving force and consequently the rate of ferrite nucleation in austenite are increased [17, 19-21].

In a study conducted by Nofal, et al. [22] on the austempered CG cast iron, the slope of the curve of retained austenite volume fraction versus time at 300 ˚C was reported to be 18˚. However, in this study, the slope of the curve for austempered samples at 300 ˚C was determined 37˚ (Fig. 1). The results demonstrate that the rate of the austempering in the Al cast iron is greater than that of the Si cast iron.

Besides, in Fig.1 the process window (Δt) of the samples austempered at 300 ˚C was determined to be about 90 minutes, Also, the process window at the austempering temperature of 400 ˚C was observed to be 30 minutes. while Desimoni [16] has shown that the process window for the Si cast iron at an austempering temperature of 300 ˚C is about 15 minutes and the process window for the austempered Si cast iron at 400 ˚C is about 5 minutes.
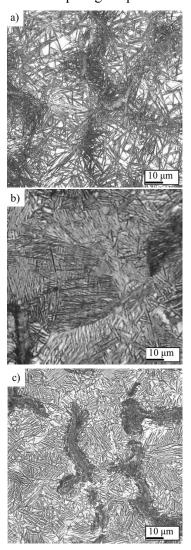
3.2. Effect of the austempering temperature on the microstructure

Microstructures of the austempered samples at 200 ˚C, 300 ˚C, and 400 ˚C for 60 minutes are shown in Fig. 2. As shown in Fig. 2a, the microstructure of the sample austempered at 200 ˚C for 60 minutes consists of an acicular appearance of bainitic ferrite and reacted stable austenite.

However, at a constant austempering time of 60 minutes, by increasing the austempering temperature to 300 ˚C and 400 ˚C the martensitic phases are removed and the microstructure becomes entirely bainitic ferrite. In addition to that, bainitic ferrite becomes thicker insofar as they are turned into the forms of planes (upper bainitic ferrite) at the austempering temperature of 400 ˚C.

Fig. 2. OM images of samples austenitized at 900 ˚C for 120 minutes and austempered at
(a). 200 ˚C (b). 300 ˚C (c). 400 ˚C for 60 min showing reacted stable austenite and bainitic ferrite.

Fig. 1. The volume fraction of retained austenite for samples austempered at 200 ˚C, 300 ˚C, and 400 ˚C.
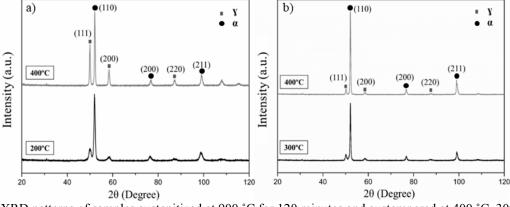
At low austempering temperatures, due to the high difference between austenitizing temperature and austempering temperature, the driving force for nucleation of bainitic ferrite is also high. Thus, this phase considerably nucleates. On the other hand, because of the low austempering temperature, carbon diffusion occurs slowly so that reduces the growth rate of the bainitic ferrite. For this reason, when the temperature is at 200 ˚C, many of the bainitic ferrites had been nucleated haven not grown much laterally. Hence, as is clears in Fig. 2a, fine formation of acicular ferrite results in the formation of lower bainitic ferrite. The low diffusion rate of the carbon also may cause transition carbide formation in acicular ferrite [15]. Moreover, at the austempering temperature of 200°C, the lower amounts of the carbon in the alloy lead to the formation of the reacted stable austenite with higher levels of carbon, and it also increases the martensite formation temperature (Ms). According to Fig. 3, it can be deduced that increasing austempering temperature and consequently reducing the temperature
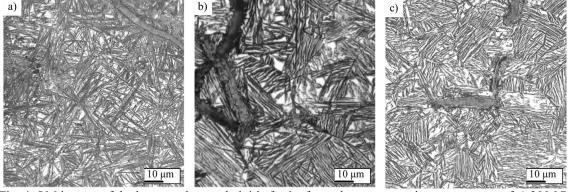
difference between austenitizing temperature and austempering temperature, decreases nucleation rate bainitic ferrite. Since the peaks attributed to Fe_xC_y carbide were not found in the XRD patterns, it can be concluded that the amount of this carbide is very low. Referring to the below equation, the volume fraction of the graphite in the alloy is determined as:

$$V_G + V\gamma + V_\alpha + V_{carbide} = 1 \qquad (1)$$

As shown in Fig.4b and Fig. 1, the microstructure has become fully bainitic ferritic. The microstructure of the samples austempered at 300 ˚C also consists of the lower bainitic ferrite phase. At the austempering temperature of 400 ˚C, the upper bainitic ferrite has formed due to the significant increase in carbon diffusion rate and a decrease in the driving force of lower bainitic ferrite nucleation. It is evident in Fig. 4c, that the upper bainitic ferrite has formed in the form of planes. The change in the morphology of bainitic ferrite from lower to upper because of the increase in temperature from 300 ˚C to 400 ˚C is obvious in Fig. 4.

Fig. 3. XRD patterns of samples austenitized at 900 ˚C for 120 minutes and austempered at 400 ˚C, 300 ˚C and 200 ˚C for a) 5 and b) 180 min.

Fig. 4. OM images of the lower and upper bainitic ferrite formed at austempering temperature of a) 200 ˚C, b) 300 ˚C and c) 400 ˚C for 180 min.
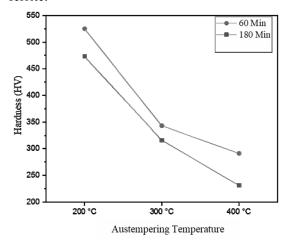
3.3. Effect of austempering temperature on the hardness

The changes in the hardness of samples with regards to the austempering temperature in two different austempering times (60 and 180 minutes) are shown in Fig. 5. Presence of the lower bainitic microstructure with an acicular appearance of bainitic ferrite and retained austenite and possibly the very fine carbides in the microstructure have caused an increase in resistance against dislocations movement and, as a result of that, have led to such a high value of hardness in these two samples.

As mentioned before, by increasing the austempering temperature, the rate of carbon diffusion into austenite is increased, and the high carbon austenite which is thermally and mechanically stable is formed. Besides, the Ms temperature is decreased. Also, at the higher austempering temperature, the rate of bainitic ferrite nucleation decreases, and on the contrary, its growth rate rises. Therefore, the number of the lower bainitic ferrite and austenite layers are reduced while their width is extended.

By increasing the austempering temperature to 300 ˚C, the hardness value reduces to 343 HV. The reasons behind this behavior include the removal of the martensite from the microstructure and thickening of the bainitic ferrite existing in the bainitic microstructure. The lowest hardness value was obtained at 400 ˚C, which was due to the absence of martensite (a hard phase) and the microstructure change from the lower bainitic ferrite to the upper bainitic ferrite.

Fig. 5. Effect of the austempering temperature on the hardness of the samples austempered for 60 and 180 min.

3.4. Effect of the austempering time on the microstructure

Because austempering transformation is based on the nucleation and growth processes, and due to its two-step nature, it is expected that at a proper austempering temperature, more carbon atoms diffuse from bainitic ferrite into the austenite by increasing the austempering time. Also, the reacted stable austenite located among the acicular ferrite becomes richer from carbon until they reach a thermally and then mechanically stable state. Eventually, as high-carbon reacted austenite decomposes to the acicular ferrite and carbide, the second step of the process starts.

Fig. 6 shows the microstructural changes in the samples austempered at 300 ˚C. Regarding the results of the examinations carried out on the austempered samples at 300 ˚C, it can be concluded that the austempering time of 5 minutes is at the first stage of the process. However, according to Fig. 1 and Fig. 2, the austempering times of 30, 60, and 120 are considered in the window process, and also the second stage starts at 120 minutes of austempering time.

Based on the microstructure of the samples, hardness values shown in Fig. 8, and also the volume fracture of austenite, it seems that at the austempering temperature of 400 ˚C, 5 minutes of austempering is considered as the first stage of the process. Besides, austempering times of 30 up to 60 minutes are in the window process. Eventually, the second stage of the austempering starts after 60 minutes of austempering time.

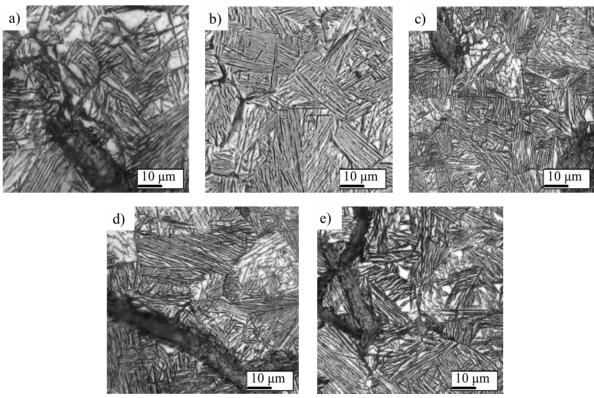### 3.5. Effect of the austempering time on the hardness

Fig. 7 shows the hardness values of the samples versus the time of austempering at different temperatures. It can be seen that at end of the first stage of austempering (30 minutes), the hardness notably decreases. After that, during the window process, by increasing austempering time and formation of acicular ferrite along with the increase of carbon in reacted stable austenite, the level of hardness has remained constant. Considering Fig. 7, the maximum hardness of each sample was obtained at the austempering time of 5 minutes.

At the austempering temperature of 300 ˚C and 200 ˚C, the hardness changes, volume fracture of

austenite, and microstructure indicate that at this temperature, by increasing austempering time from 5 to 30 minutes, the second stage of austempering has not started yet (Fig. 1, 6 and 7). On the other hand, at the austempering temperature of 200 ˚C after 60 minutes, the hardness decreases due to the start of the second stage.

The hardness of the Al cast iron is higher than Si cast iron. In the case of Si cast irons, the maximum hardness of 600 HV is obtained by austempering at 300 ˚C for 5 minutes [21]. But, in the present study at similar conditions, this value is reported to be 680 HV for the Al cast iron.

Fig. 6. Microstructures of the austempered samples at 300 ˚C for a) 5, b) 30, c) 60, d) 120, and e) 180 min austempering time showing reacted stable austenite and bainitic ferrite.
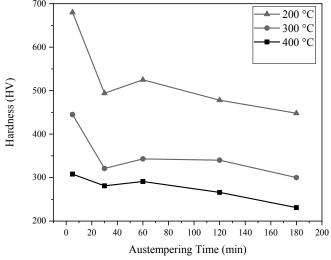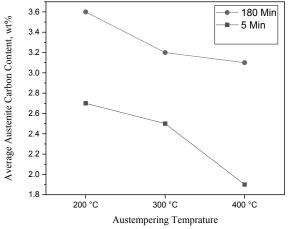

Fig. 7. Changes in the hardness values of Fe-3.4C-4.8Al alloy at different austempering temperatures and times.

A. Kazazi, S. M. Montazeri and S. M. A. Boutorabi

3.6. Effect of the austempering time on the carbon content of the retained austenite

Fig. 8 shows changes in the carbon content of the retained austenite versus austempering time at three temperatures of 200 ˚C, 300 ˚C, and 400 ˚C. The content of the carbon in the retained austenite can be seen to increase with austempering time. The reason is high carbon rejection into the surrounding austenite due to the high rate of ferrite nucleation. According to Fig. 8, in the case of the sample austempered at 200 ˚C, the carbon amount of the retained austenite increased from 2.7 wt% in the austempering time of 5 minutes to 3.5 wt% in the 180 minutes of austempering.

It can also be seen that the carbon content of retained austenite decreases with increasing austempering temperature. Therefore, for given initial carbon content, more acicular ferrite forms and less retained austenite remains at the end of the first reaction. The decrease in carbon content at high austempering temperature is accompanied by a decrease in retained austenite. As austempering temperature decreases, the retained austenite phase dissolves an increasing amount of carbon.

Maximum amount of carbon in austenite reaches 3.5 wt% at 200 ˚C austempering temperature and 180 minutes of the process; whereas, the minimum value was 2.0 wt% at the austempering temperature of 400 ˚C and time of 5 minutes. The maximum value of retained austenite carbon content in CG Al iron, 2.4 %, is also higher than that of CG Si iron. The maximum value of retained austenite carbon content reported in the literature for Si iron is 1.8

The %. This confirms the stronger graphitizing effect of Al compared with Si. This characteristic is thought to result from the better ability of Al to suppressing the formation of the carbide phase normally associated with bainitic transformation. In addition, the stronger graphitizing effect of Al on suppressing carbide formation increases the retained austenite carbon content to a high level [23].

3.7. Retained austenite

The most important product of the bainitic reaction is retained austenite, the volume, and characteristics of which govern the final mechanical properties of the iron. Unreacted or untransformed austenite is the main stage I constituent.

According to Fig. 4, reacted stable austenite can be seen close to the acicular ferrite structures. The presence of the unreacted retain austenite at the vicinity of vermicular graphite is shown in Fig. 9.
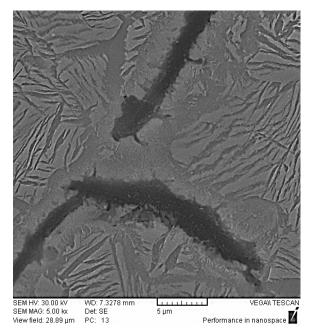

Fig. 9. SEM image of sample austempered at 400 ˚C for 30 minutes showing the presence of unreacted austenite phase around the vermicular graphite.

4. CONCLUSION

The presence of 4.8 wt% Al instead of the Si was seen to lead to the difference between the Al and Si cast irons in the effect of temperature and time variables on the kinetics of austempering. The austempering parameters had considerable

Fig. 8. Effect of the austempering time on the carbon amount of the retained austenite.

effects on the microstructure and austempering kinetics of the Fe-3.2C-4.8Al CG cast iron. The following points were concluded:

1. The lower bainitic ferrite formed in the samples austempered at 200 ˚C and 300 ˚C. By increasing the austempering temperature to 400 ˚C, the bainitic ferrite morphology changed to the upper bainitic ferrite.

2. Generally, the hardness of the austempered sample decreased as the temperature was raised. The hardness of the austempered samples at 200 ˚C, 300 ˚C, and 400 ˚C was in the range of 473 to 680 HV, 316 to 445 HV, and 231 to 308 HV, respectively.

3. The austempering time of 5 minutes at all the three temperatures (200 ˚C, 300 ˚C, and 400 ˚C) was in the time range of the first step of austempering. By the beginning of the second stage, hardness decreased slightly. At austempering temperatures of 200 and 300 ˚C, the second stage started after 120 minutes and for the austempering temperature of 400 ˚C, the second stage started after 60 minutes.

4. The hardness value of the austempered sample at 200 ˚C for 5 minutes was higher than the sample that was cooled in water after austenitizing and contained martensite in its microstructure. Hardness increased from 530 HV for the quenched sample to 680 HV for the austempered sample.

REFERENCES

1. Palm, M., Stein, F. and Dehm, G., Iron Aluminides. Annu. Rev. Mater. Res., 2019, 49, 1–30.

2. Aguado, E., Ferrer, M., Larrañaga, P., Stefanescu, D. M. and Suárez, R., The Effect of the Substitution of Silicon by Aluminum on the Properties of Lamellar Graphite Iron. Int. J. Met., 2019, 13, 1–10.

3. Defrancq, C., van Feghem, J. and Desy, A. A., Study of the inoculation of gray cast irons from the Fe–C–Al system; development of a new flake graphite cast iron with very high strength. 36th Int. Foundry Congr. Belgrade, Serbia 1969.

4. Boutorabi, S. M. A., Salehi, M., Young, J. M. and Kondic, V., The tribological behaviour aluminium cast iron. Wear., 1993, 165, 19–24.

5. Zandira, M. and Boutorabi, S. M. A., Fracture Characteristics of Austempered Spheroidal Graphite Aluminum Cast Irons. J. Iron Steel Res. Int., 2010, 17, 31–5.

6. Erfanian-Naziftoosi, H. R., Haghdadi, N. and Kiani-Rashid, A. R., The Effect of Isothermal Heat Treatment Time on the Microstructure and Properties of 2 . 11 % Al Austempered Ductile Iron. J Mater Eng Perform., 2012, 21, 1785–92.

7. Martinez, F. and Stefanescu D., Compacted / Vermicular Graphite Cast Irons in the Fe-C-AI System. Am. Foundry Soc. Trans., 1982, 90, 39–46.

8. Kashani, S. M. M. and Boutorabi S. M. A., As-Cast Acicular Ductile Aluminum Cast Iron. J. Iron Steel Res. Int., 2009, 16, 23–8.

9. Soiński, M. S., Jakubus, A., Kordas, P. and Skurka, K., The Effect of Aluminium on Graphitization of Cast Iron Treated with Cerium Mixture. Arch. Foundry Eng., 2014, 14, 95–100.

10. Perez, M. J., Cisneros, M. M., Almanza, E. and Haro, S., Kinetic Study of the Austempering Reactions in Ductile Irons. J. Mater. Eng. Perform., 2012, 21, 2460–6.

11. Rundman, K. B., Moore, D. J., Hayrynen, K. L., Dubensky, W. J. and Rouns, T. N., The Microstructure and Mechanical Properties of Austempered Ductile Iron. J. Heat Treat., 1988, 5, 79–95.

12. Meier, L., Hofmann, M., Saal, P., Volk, W. and Hoffmann, H., ScienceDirect In-situ measurement of phase transformation kinetics in austempered ductile iron. Mater Charact., 2013, 85, 124–33.

13. Laneri, K., Bruna, P. and Crespo, D., Microstructural characterisation and kinetics modelling of vermicular cast irons. Mater. Sci. Technol., 2008, 24, 1214–21.

14. Sidjanin, L., Smallman, R. and Young, J., Electron microstructure and mechanical properties of silicon and aluminium ductile irons. Acta Metall Mater., 1994, 42, 3149–56.

15. Sidjanin, L., Smallman, R. E. and Boutorabi, S. M. A., Microstructure and fracture of aluminium austempered ductile iron investigated using electron microscopy, Mater. Sci Technol., 1994, 10, 711–20.

16. Desimoni, J., Austempering Transformation Kinetics of Compacted Graphite Cast Irons Obtained by Mössbauer Spectroscopy Hyperfine Interact., 2001, 134, 93–102.

17. Kiani-rashid, A. R. and Edmonds, D. V., Microstructural characteristics of Al-alloyed austempered ductile irons. J Alloys Compd., 2009, 477, 391–8.

18. Arft, M., Klocke, F. and Lung, D., Evaluation of the machining aspects of austempered ductile iron. Int J Met., 2012, 6, 35–42.

19. Shayesteh-zeraati, A., Naser-zoshki, H. and Kiani-rashid, A. R., Microstructural and mechanical properties (hardness) investigations of Al-alloyed ductile cast iron, J. Alloys Compd., 2010, 500, 129–33.

20. Benam, A. S., Effect of alloying elements on austempered ductile iron (ADI) properties and its process: Review. China Foundry., 2015, 12, 54–70.

21. Bayati, H., Rimmer, A. L. and Elliott, R., The austempering kinetics and processing window in an austempered , low-manganese compacted- graphite cast iron, Cast. Met., 1994, 7, 11–24.

22. Ramadan, M., Nofal, A. A., Elmahalawi, I. and Abdel-Karim, R., Comparison of austempering transformation in spheroidal graphite and compacted graphite cast irons, Int. J. Cast Met. Res., 2006, 19, 151–5.

23. Laneri, K. F., Desimoni, J., Mercader, R. C., Gregorutti, R. W. and Sarutti, J. L., Thermal Dependence of Austempering Transformation Kinetics of Compacted Graphite Cast Iron, Metal Mater. Trans. A., 2001, 32, 51–8.

54